Polyhedron 31 (2012) 319–331

Contents lists available at SciVerse ScienceDirect

Polyhedron

journal homepage: www.elsevier.com/locate/poly

Molecular and spectroscopic properties of hydridecarbonyl ruthenium complexes with pyrazine carboxylic acid ligands

J.G. Małecki [a,*], T. Groń [b], H. Duda [b]

[a] Department of Crystallography, Institute of Chemistry, University of Silesia, ul. Szkolna 9, 40-006 Katowice, Poland
[b] Institute of Physics, University of Silesia, ul. Uniwersytecka 4, 40-007 Katowice, Poland

ARTICLE INFO

Article history:
Received 30 July 2011
Accepted 17 September 2011
Available online 4 October 2011

Keywords:
Ruthenium hydridocarbonyl complexes
Pyrazine carboxylic acid
Ruthenium(III)/ruthenium(II) dinuclear complexes
Absorptions and emissions electronic spectra
DFT
Dynamic magnetic susceptibility

ABSTRACT

The hydride carbonyl ruthenium(II) [RuH(CO)(pyzCOO)(PPh_3)$_2$] (**1**), [RuH(CO)(pyz-2,3-COO[CH_3])(PPh_3)$_2$]·H_2O (**2**) and dinuclear Ru(II)/Ru(III) [RuH(CO)(PPh_3)(pyz-2,3-COO)Ru(CO)Cl_2(PPh_3)$_2$] (**3**) complexes were synthesized and characterized by IR, ^{1}H, ^{31}P NMR, UV–Vis spectroscopy and X-ray crystallography. The experimental studies were complemented by quantum chemical calculations, which were used to identify the nature of the interactions between the ligands and the central ion, and the orbital composition in the frontier electronic structure. Based on a molecular orbital scheme, the calculated results allowed the interpretation of the UV–Vis spectra obtained at an experimental level. The luminescence property of the complex **2** was determined. The ac magnetic susceptibility measurements showed a residual magnetism evidenced by the small values of the molar susceptibility, not exceeding 0.5 emu/mol at 2 K, a lack of a Curie-Weiss region and weak magnetic interactions below 20 K.

1. Introduction

Ruthenium hydride complexes containing carbonyl and triarylphosphine ligands are interesting due to their reactivity and efficiency as catalysts in a wide spectrum of reactions [1–6]. On the other hand, complexes of ruthenium containing π-acceptor nitrogen-bearing ligands, especially *N*-heteroaromatic ligands, have been widely studied as systems for the conversion of energy. Studies on the synthesis and characterization of ruthenium complexes containing *N*-heteroaromatic ligands have received considerable recent attention, owing to their interesting photophysical and photochemical properties. The azine ligands have energetically low lying π-antibonding orbitals, which can accept electrons from filled metal d orbitals. As a consequence, they can exhibit charge transfer bands with interesting spectroscopic properties in the visible region [7]. Ligands containing a pyrazine ring are widely studied and their π-donor properties are interesting. Their combination with other donor atoms should in principle afford complexes with tunable spectroscopic properties [8–10]. The hydride ligand – a powerful σ-donor – is found to be very efficient at compensating for electron deficiency at a metal central ion in complexes. The "trans effect" of the H^- ligand and the interaction between carbonyl and donor ligands (such as carboxyl or chloride) in *trans* positions to one another are stabilizing factors which explain the stability of these complexes [11], which are interesting due to theirs properties. Pyrazine derivatives can act as exo-bidentate ligands. This feature makes pyrazine and its derivatives intriguing ligands for the study of dinuclear or multinuclear mixed-valence and mixed-metal complexes [12–14].

Here an experimental and quantum chemical study of ruthenium hydridocarbonyl complexes with pyrazine carboxylic acid ligands is reported. The quantum chemical study includes characterization of the molecular and electronic structures of the complexes by analysis of the optimized molecular geometries and electronic populations using the natural bond orbitals scheme. The latter was used to identify the nature of the interactions between the ligands and the central ion. The calculated density of states shows the interactions and influences the orbital composition in the frontier electronic structure. Time dependent density functional theory (TD-DFT) was finally used to calculate the electronic absorption spectra. Based on a molecular orbital scheme, these results allow the interpretation of the UV–Vis spectra obtained at an experimental level. The complexes reported in this paper combine the interest in ruthenium hydride carbonyl coordination compounds and complexes containing *N*-heterocyclic ligands [15–23]. Additionally the magnetic properties of a dinuclear complex were measured.

2. Experimental

All reagents used for the synthesis of the complexes are commercially available and have been used without further purification. The

* Corresponding author.
E-mail address: gmalecki@us.edu.pl (J.G. Małecki).

0277-5387/$ - see front matter © 2011 Elsevier Ltd. All rights reserved.
doi:10.1016/j.poly.2011.09.032

[RuHCl(CO)(PPh_3)$_3$] complex was synthesized according to the literature method [24].

2.1. Synthesis of [RuH(CO)(pyzCOO)(PPh_3)$_2$] (**1**), [RuH(CO)(pyz-2,3-COO[CH_3])(PPh_3)$_2$]·H_2O (**2**) and [RuH(CO)(PPh_3)(pyz-2,3-COO)Ru(CO)Cl_2(PPh_3)$_2$] (**3**)

The complexes **1** and **2** were synthesized in the reaction between [RuHCl(CO)(PPh_3)$_3$] (0.1 g, 1×10^{-4} mol) and pyrazine-2-carboxylic acid (pyzCOO) or pyrazine-2,3-dicarboxylic acid (pyz-2,3-COO) in methanol solution (100 cm^{-3}). The reaction with pyrazine-2,3-dicarboxylic acid was also performed in acetone and complex **3** was obtained. A mixture of the compounds was refluxed in methanol or acetone for 4 h. After this time, it was cooled and filtered. Crystals suitable for X-ray crystal analysis were obtained by slow evaporation of the reaction mixtures.

1: Yield 62%. IR (KBr, cm^{-1}): 3048 ν_{ArH}; 1973 $\nu_{(CO)}$; 1928 $\nu_{(Ru-H)}$; 1655 $\nu_{(C=N;\ C=C)}$; 1580 $\nu_{as(COO)}$; 1479 $\delta_{(C-CH\ in\ the\ plane)}$; 1434 $\nu_{Ph(P-Ph)}$; 1334 $\nu_{s(COO)}$; 1092 $\delta_{(C-CH\ in\ the\ plane)}$; 745 $\delta_{(C-C\ out\ of\ the\ plane)}$; 694 $\delta_{(C-C\ in\ the\ plane)}$; 517 $\nu_{(P-Ph+P-Ru)}$. UV–Vis (methanol, nm (logε): 361.5 (1.17), 316.2 (1.90), 273.1 (2.86), 224.2 (sh), 210.6 (4.82). ^{1}H NMR (400 MHz, $CDCl_3$) δ (ppm): 8.39 (s, H_{pyz}), 7.90 (d, J = 2.9 Hz, 2H_{pyz}), 7.83–7.49 (m, PPh_3), −9.51 (t_{Ru-H}, J = 19.6 Hz). ^{31}P NMR ($CDCl_3$) δ (ppm): 43.85 (s, PPh_3).

2: Yield 73%. IR (KBr, cm^{-1}): 3447 ν_{OH}; 3055 ν_{ArH}; 1958 $\nu_{(CO)}$; 1922 $\nu_{(Ru-H)}$; 1749 (H_2O); 1644 $\nu_{(C=N;\ C=C)}$; 1569 $\nu_{as(COO)}$; 1479 $\delta_{(C-CH\ in\ the\ plane)}$; 1437 $\nu_{Ph(P-Ph)}$; 1339 $\nu_{s(COO)}$; 1299 $\nu_{s(COO)}$; 1093 $\delta_{(C-CH\ in\ the\ plane)}$; 795 $\delta_{(C-C\ out\ of\ the\ plane)}$; 693 $\delta_{(C-C\ in\ the\ plane)}$; 519 $\nu_{(P-Ph+P-Ru)}$. UV–Vis (methanol, nm (logε): 360.0 (1.26), 310.2 (1.79), 274.0 (2.32), 267.0 (2.41), 232.0 (sh), 211.8 (4.92). ^{1}H NMR (400 MHz, $CDCl_3$) δ (ppm): 7.88 (d, 2H_{pyz}), 7.76–7.23 (m, PPh_3), 3.83 (s, CH_3), 1.56 (s, H_2O), −9.57 (t_{Ru-H}, J = 19.4 Hz). ^{31}P NMR ($CDCl_3$) δ (ppm): 44.04 (s, PPh_3).

3: Yield 73%. IR (KBr, cm^{-1}): 3045 ν_{ArH}; 1947, 1943 $\nu_{(CO)}$; 1923 $\nu_{(Ru-H)}$; 1593 $\nu_{(C=N;\ C=C)}$; 1559 $\nu_{as(COO)}$; 1480 $\delta_{(C-CH\ in\ the\ plane)}$; 1433 $\nu_{Ph(P-Ph)}$; 1359 $\nu_{s(COO)}$; 1219, 1155 $\nu_{(pyz\ ring)}$; 998 $\delta_{(CHpyz\ out\ the\ plane)}$; 843 $\delta_{(Ru-pyz\ COO\ in\ the\ plane)}$; 749 $\delta_{(Ru-pyz\ COO\ out\ of\ the\ plane)}$; 695 $\delta_{(pyz\ ring\ out\ of\ the\ plane)}$; 516 $\nu_{(N-Ru)}$. UV–Vis (dichloromethane, nm (logε): 603.0 (1.41), 570.0 (1.69), 515.0 (1.67), 450.2 (1.22), 371.5 (1.19), 298.4 (2.13), 212.6 (4.97). ^{1}H NMR (400 MHz, $CDCl_3$) δ (ppm): 7.75 (dd, J = 17.5, 7.1 Hz, H_{pyz}), 7.72–7.21 (m, PPh_3), −9.529 (t_{Ru-H}, J = 19.3 Hz). ^{31}P NMR ($CDCl_3$) δ (ppm): 47.12 (s), 43.16 (s, PPh_3), 26.17 (s, (Ru(2)PPh_3).

2.2. Physical measurements

Infrared spectra were recorded on a Nicolet Magna 560 spectrophotometer in the spectral range 4000–400 cm^{-1} using KBr pellets. Electronic spectra were measured on a Lab Alliance UV–Vis 8500 spectrophotometer in the range of 900–180 nm in methanol solution. The ^{1}H and ^{31}P NMR spectra were obtained at room temperature in $CDCl_3$ using a Bruker 400 MHz spectrometer. Luminescence measurements were made on methanolic solutions with an F-2500 FL spectrophotometer at room temperature. Dynamic (ac) magnetic susceptibility was measured with the aid of a Quantum Design System (MPMS XL) and recorded in the temperature range 2–300 K and at an internal oscillating magnetic field H_{ac} = 3.9 Oe with an internal frequency f = 300 Hz.

2.3. Computational methods

The calculations were carried out using the GAUSSIAN09 [25] program. Molecular geometries of the singlet ground state of complexes **1** and **2**, and the doublet state of the dimeric complex **3** were fully optimized in the gas phase at the B3LYP/DZVP level of theory. [26,27] For each compound a frequency calculation was carried out, verifying that the optimized molecular structure obtained

Table 1
Crystal data and structure refinement details of the complexes [RuH(CO)(pyzCOOH)(PPh_3)$_2$] (**1**), [RuH(CO)(pyz-2,3-COO[CH_3])(PPh_3)$_2$]·H_2O (**2**) and [Ru_2HCl_2(PPh_3)$_3$(pyz-2,3-COO)] (**3**).

	1	**2**	**3**
Empirical formula	$C_{42}H_{34}N_2O_3P_2Ru$	$C_{44}H_{36}N_2O_5P_2Ru$, H_2O	$C_{62}H_{48}Cl_2N_2O_6P_3Ru_2$
Formula weight	777.72	853.77	1282.97
Temperature (K)	295.0 (2)	295.0 (2)	295.0 (2)
Crystal system	monoclinic	monoclinic	triclinic
Space group	$P2_1/n$	$P2_1/n$	$P\bar{1}$
Unit cell dimensions			
a (Å)	10.196(2)	14.8922(5)	12.4781(6)
b (Å)	15.426(3)	15.5794(5)	13.8575(7)
c (Å)	22.871(5)	17.6954(7)	17.7429(8)
α (°)	90	90	69.534(4)
β (°)	97.51(3)	93.385(3)	87.090(5)
γ (°)	90	90	83.246(4)
Volume (Å^3)	3566.3(12)	4098.4(2)	2854.3(2)
Z	4	4	2
Calculated density (mg/m^3)	1.448	1.384	1.493
Absorption coefficient (mm^{-1})	0.572	0.513	0.760
F (000)	1592	1752	1298
Crystal dimensions (mm)	0.09 × 0.07 × 0.03	0.37 × 0.32 × 0.06	0.18 × 0.12 × 0.05
θ range for data collection (°)	3.32 to 25.05	3.65 to 25.05	3.40 to 25.05
Index ranges	$-12 \leqslant h \leqslant 12$	$-17 \leqslant h \leqslant 17$	$-14 \leqslant h \leqslant 14$
	$-15 \leqslant k \leqslant 18$	$-18 \leqslant k \leqslant 18$	$-16 \leqslant k \leqslant 16$
	$-27 \leqslant l \leqslant 27$	$-21 \leqslant l \leqslant 20$	$-21 \leqslant l \leqslant 21$
Reflections collected	19891	38929	28425
Independent reflections (R_{int})	6294 (0.0488)	7237 (0.0331)	10056 (0.0684)
Data/restraints/parameters	6294/0/455	7237/0/514	10056/0/698
Goodness-of-fit on F^2	0.970	1.058	0.938
Final R indices [$I > 2\sigma(I)$]	R_1 = 0.0374	R_1 = 0.0320	R_1 = 0.0715
	wR_2 = 0.0720	wR_2 = 0.0772	wR_2 = 0.1364
R indices (all data)	R_1 = 0.0697	R_1 = 0.0446	R_1 = 0.1404
	wR_2 = 0.0784	wR_2 = 0.0830	wR_2 = 0.1594
Largest difference in peak and hole (e Å^{-3})	0.742 and −0.536	0.514 and −0.408	1.007 and −1.010

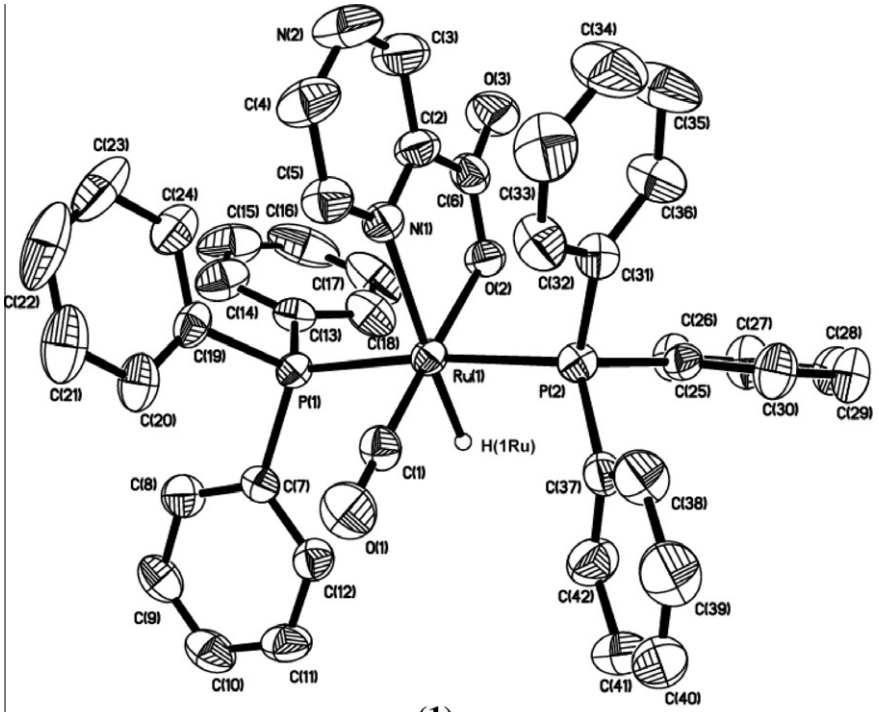

(1)

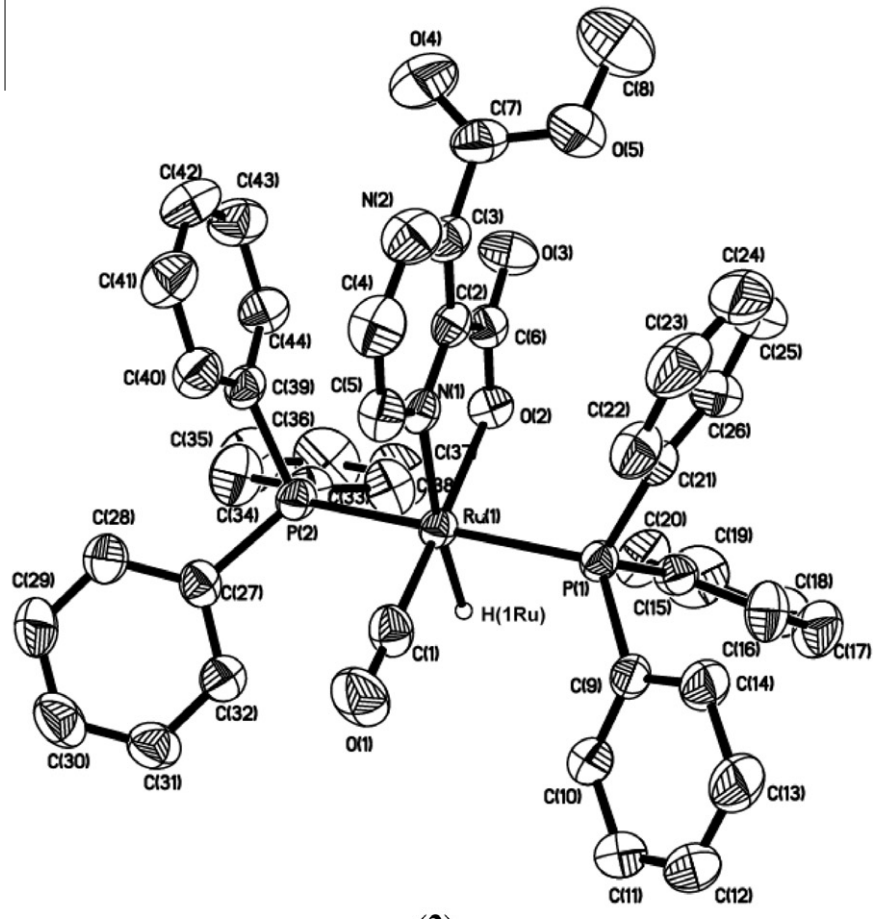

(2)

Fig. 1. ORTEP drawings of the complexes [RuH(CO)(pyzCOOH)(PPh_3)$_2$] (**1**), [RuH(CO)(pyz-2,3-COO[CH_3])(PPh_3)$_2$]·H_2O (**2**) and [Ru_2HCl_2(PPh_3)$_3$(pyz-2,3-COO)] (**3**) with 50% probability displacement ellipsoids. Hydrogen atoms (except Ru–H) and the water molecule in complex (**2**) are omitted for clarity.

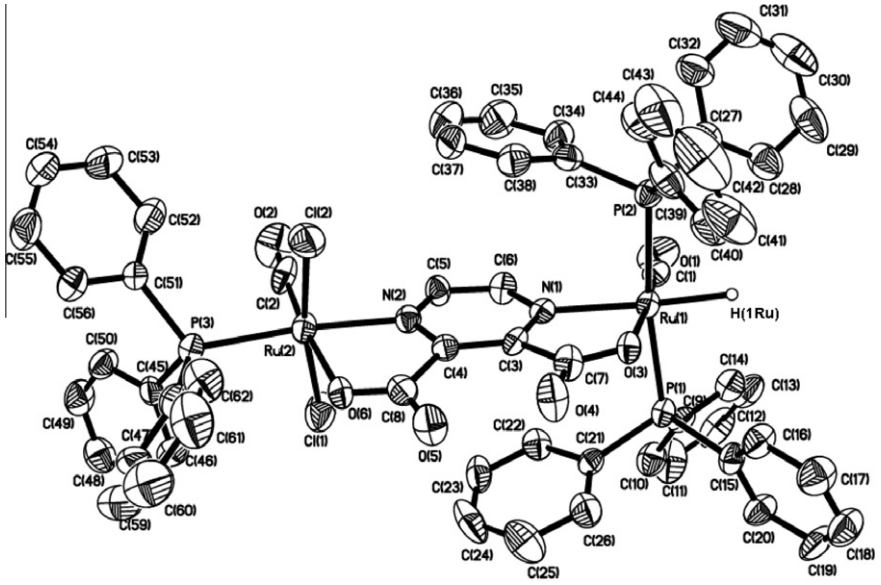

(3)

Fig. 1 (*continued*)

corresponds to an energy minimum, thus only positive frequencies were expected. The DZVP basis set [28] with f functions and with exponents of 1.94722036 and 0.748930908 was used to describe the ruthenium atom, and the basis set used for the lighter atoms (C, N, O, P, H, Cl) was 6-31G with a set of "d" and "p" polarization functions. The TD-DFT (time dependent density functional theory) method [29] was employed to calculate the electronic absorption spectra of the complexes in the solvent PCM (Polarizable Continuum Model) model. In this work 90 singlet excited states were calculated as vertical transitions for the complexes. A natural bond orbital (NBO) analysis was also made for all the complexes using the NBO 5.0 package [30] included in GAUSSIAN09. Natural bond orbitals are orbitals localized on one or two atomic centers that describe molecular bonding in a manner similar to a Lewis electron pair structure, and they correspond to an orthonormal set of localized orbitals of maximum occupancy. NBO analysis provides the contribution of atomic orbitals (s, p, d) to the NBO σ and π hybrid orbitals for bonded atom pairs. In this scheme, three NBO hybrid orbitals are defined, bonding orbital (BD), lone pair (LP) and core (CR), which were analyzed on the atoms directly bonded to or presenting some kind of interaction with the ruthenium atom. The contribution of a group (ligands, central ion) to a molecular orbital was calculated using Mulliken population analysis. GaussSum 2.2 [31] was used to calculate group contributions to the molecular orbitals and to prepare the partial density of states (DOS) spectra. The DOS spectra were created by convoluting the molecular orbital information with GAUSSIAN curves of unit height and a FWHM (*Full Width at Half Maximum*) of 0.3 eV.

2.4. Crystal structure determination and refinement

The crystals of [RuH(CO)(pyzCOO)(PPh_3)$_2$] (**1**), [RuH(CO)(pyz-2,3-COO[CH_3])(PPh_3)$_2$]·H_2O (**2**) and [RuH(CO)(PPh_3)(pyz-2,3-CO-O)Ru(CO)Cl_2(PPh_3)$_2$] (**3**) were mounted in turn on an Xcalibur, Atlas, Gemini Ultra Oxford Diffraction automatic diffractometer equipped with a CCD detector, and were used for data collection. X-ray intensity data were collected with graphite monochromated Mo Kα radiation (λ = 0.71073 Å) at temperature of 295.0(2) K, with the ω scan mode. Ewald sphere reflections were collected up to 2θ = 50.10°. The unit cell parameters were determined from least-squares refinement of the setting angles of 7523, 12218 and 10395 strongest reflections for complexes **1**, **2** and **3**, respectively. Details concerning crystal data and refinement are gathered in Table 1. Lorentz, polarization and empirical absorption corrections using spherical harmonics implemented in SCALE3 ABSPACK scaling algorithm [32] were applied. The structure was solved by the Patterson method and subsequently completed by difference Fourier recycling. All the non-hydrogen atoms were refined anisotropically using the full-matrix, least-squares technique. The hydrogen atoms were found from the difference Fourier synthesis after four cycles of anisotropic refinement, and were refined as "riding" on the adjacent carbon atom with individual isotropic temperature factor equal 1.2 times the value of equivalent temperature factor of the parent atom. The Olex2 [33] and SHELXS97, SHELXL97 [34] programs were used for all the calculations. Atomic scattering factors were those incorporated in the computer programs.

3. Results and discussion

3.1. Spectroscopic characterization of the complexes

The ^{31}P NMR spectra of the complexes [RuH(CO)(pyz-COOH)(PPh_3)$_2$] (**1**) and [RuH(CO)(pyz-2,3-COO[CH_3])(PPh_3)$_2$]·H_2O (**2**) show singlets at 43.848 and 44.038 ppm. The broadening of the signals suggests that the triphenyphosphine ligands are not in perfect *trans* positions. In the case of complex **3**, the ^{31}P NMR spectrum presents three signals at 47.122, 43.158 and 26.166 ppm. The low field signals indicate PPh_3 ligands at a ruthenium(II) central ion and the high field signal is attributed to a triphenylphosphine molecule at the Ru(III) centre. The ^{1}H NMR spectra of the complexes show a set of signals corresponding to the PPh_3 ligands. The pyrazine aromatic protons in the spectra of complexes **1** and **2** are visible as a singlet at 8.386 ppm (H(3)) and doublets due to the magnetic ortho coupling of the H(4) and H(5) protons at 7.896 ppm in **1** and 7.882 ppm in **2**. The signals are shifted compared with free pyrazine carboxylic acid (9.24, 8.91, 8.85 ppm) due to the shielding effect of the ruthenium central ion. The spectrum of complex **2** presents signals at 3.827 and 1.557 ppm that are attributed to the ester CH_3

Table 2
Selected bond lengths (Å) and angles (°) for the complexes [RuH(CO)(pyzCOOH)(PPh_3)$_2$] (**1**), [RuH(CO)(pyz-2,3-COO[CH_3])(PPh_3)$_2$]·H_2O (**2**) and [$Ru_2HCl_2(PPh_3)_3$(pyz-2,3-COO)] (**3**).

	1		**2**	
	Exp	Calc	Exp	Calc
Bond lengths (Å)				
Ru(1)–C(1)	1.814(3)	1.856	1.822(5)	1.854
Ru(1)–N(1)	2.167(2)	2.237	2.151(3)	2.240
Ru(1)–O(2)	2.113(2)	2.160	2.146(3)	2.160
Ru(1)–P(1)	2.3554(10)	2.433	2.3461(11)	2.434
Ru(1)–P(2)	2.3487(10)	2.433	2.3554(11)	2.438
Ru–H1(Ru)	1.56(3)	1.620	1.73(4)	1.620
C(1)–O(1)	1.153(4)	1.165	1.151(6)	1.165
Angles (°)				
C(1)–Ru(1)–O(2)	178.52(11)	173.40	175.76(18)	173.73
C(1)–Ru(1)–N(2)	103.68(12)	98.52	100.08(19)	99.18
O(2)–Ru(1)–N(1)	76.41(9)	74.93	75.74(12)	74.65
C(1)–Ru(1)–P(2)	89.53(10)	93.95	94.32(15)	94.04
O(2)–Ru(1)–P(2)	88.99(6)	86.06	87.24(8)	93.36
P(2)–Ru(1)–N(1)	94.68(6)	96.34	94.72(9)	96.07
P(1)–Ru(1)–C(1)	88.07(10)	88.92	92.32(15)	88.39
P(1)–Ru(1)–O(2)	93.41(6)	92.56	86.86(8)	85.50
P(1)–Ru(1)–N(1)	92.25(6)	95.96	93.92(9)	95.17
P(1)–Ru(1)–P(2)	173.03(3)	166.81	168.02(4)	167.97
C(1)–Ru(1)–H(1)	84.4(12)	91.00	84.7(13)	91.00
O(2)–Ru(1)–H(1)	95.5(12)	95.00	99.4(13)	96.00
N(1)–Ru(1)–H(1)	171.5(12)	170.00	173.5(13)	170.00
P(2)–Ru(1)–H(1)	87.8(10)	84.00	89.2(13)	85.00
P(1)–Ru(1)–H(1)	85.5(11)	83.00	81.5(13)	83.00
Ru(1)–C(1)–O(1)	178.7(3)	174.66	177.8(5)	174.93

3

	Exp	Calc		Exp	Calc
Bond lengths (Å)					
Ru(1)–C(1)	1.816(7)	1.851	Ru(2)–C(2)	1.800(8)	1.843
Ru(1)–N(1)	2.162(4)	2.232	Ru(2)–N(2)	2.123(5)	2.140
Ru(1)–O(3)	2.140(4)	2.179	Ru(2)–O(6)	2.127(4)	2.181
Ru(1)–P(1)	2.3782(18)	2.451	Ru(2)–P(3)	2.3316(17)	2.406
Ru(1)–P(2)	2.3648(17)	2.427	Ru(2)–Cl(1)	2.380(2)	2.454
Ru–H(1)	1.72(5)	1.610	Ru(2)–Cl(2)	2.3887(19)	2.457
C(1)–O(1)	1.160(8)	1.163	C(2)–O(2)	1.145(8)	1.162
Angles (°)					
C(1)–Ru(1)–O(3)	174.8(2)	174.19	C(2)–Ru(2)–N(2)	99.0(2)	97.17
C(1)–Ru(1)–N(1)	101.4(2)	100.95	C(2)–Ru(2)–O(6)	174.0(2)	172.15
O(3)–Ru(1)–N(1)	73.90(16)	73.31	N(2)–Ru(2)–O(6)	75.06(17)	75.02
C(1)–Ru(1)–P(2)	88.5(2)	89.10	C(2)–Ru(2)–P(3)	90.6(2)	91.57
O(3)–Ru(1)–P(2)	93.84(12)	92.07	N(2)–Ru(2)–P(3)	170.44(15)	171.10
N(1)–Ru(1)–P(2)	92.14(13)	93.22	O(6)–Ru(2)–P(3)	95.40(11)	96.26
C(1)–Ru(1)–P(1)	93.0(2)	94.30	C(2)–Ru(2)–Cl(1)	89.7(2)	90.70
O(3)–Ru(1)–P(1)	85.45(12)	85.52	N(2)–Ru(2)–Cl(1)	84.06(14)	86.39
N(1)–Ru(1)–P(1)	95.63(13)	95.64	O(6)–Ru(2)–Cl(1)	89.06(14)	88.04
P(2)–Ru(1)–P(1)	171.68(6)	169.73	P(3)–Ru(2)–Cl(1)	96.71(6)	95.22
C(1)–Ru(1)–H(1)	89.6(17)	89.00	C(2)–Ru(2)–Cl(2)	95.7(2)	94.83
O(3)–Ru(1)–H(1)	95.4(17)	97.00	N(2)–Ru(2)–Cl(2)	86.87(14)	86.72
N(1)–Ru(1)–H(1)	166.6(18)	170.00	O(6)–Ru(2)–Cl(2)	84.63(13)	85.63
P(2)–Ru(1)–H(1)	80.5(17)	84.00	P(3)–Ru(2)–Cl(2)	91.55(7)	90.89
P(1)–Ru(1)–H(1)	91.3(17)	87.00	Cl(1)–Ru(2)–Cl(2)	170.05(7)	171.65
Ru(1)–C(1)–O(1)	177.0(6)	176.32	Ru(2)–C(2)–O(2)	175.0(7)	174.74

Table 3
Hydrogen bonds for the complexes [RuH(CO)(pyzCOOH)(PPh_3)$_2$] (**1**), [RuH(CO)(pyz-2,3-COO[CH_3])(PPh_3)$_2$]·H_2O (**2**) and [$Ru_2HCl_2(PPh_3)_3$(pyz-2,3-COO)] (**3**) (Å and °).

D–H···A	d(D–H)	d(H···A)	d(D···A)	<(DHA)
1				
C(26)–H(26)···O(2)	0.93	2.41	3.123(4)	133.3
C(18)–H(18)···O(2)	0.93	2.51	3.021(4)	114.8
2				
C(8)–H(8A)···O(1) #1	0.96	2.39	3.252(9)	149.1
C(31)–H(31)···O(4) #2	0.93	2.60	3.303(7)	133.0
C(35)–H(35)···O(6) #3	0.93	2.58	3.490(8)	167.6
C(38)–H(38)···O(2)	0.93	2.51	3.157(6)	128.0
3				
C(5)–H(5)···O(2) #4	0.93	2.57	3.173(9)	122.9
C(16)–H(16)···O(3)	0.93	2.42	3.196(8)	140.6
C(44)–H(44)···Cl(1)	0.93	2.74	3.181(7)	109.7
C(60)–H(60)···Cl(2)	0.93	2.77	3.604(8)	149.2

Symmetry transformations used to generate equivalent atoms: #1 1/2 − *x*, −1/2 + *y*, 1/2 − *z*; #2, −1/2 + *x*,3/2 − *y*, −1/2 + *z*; #3 1 − x, 1 − y, −*z*; #4 1 − *x*, 1 − *y*, 1 − *z*.

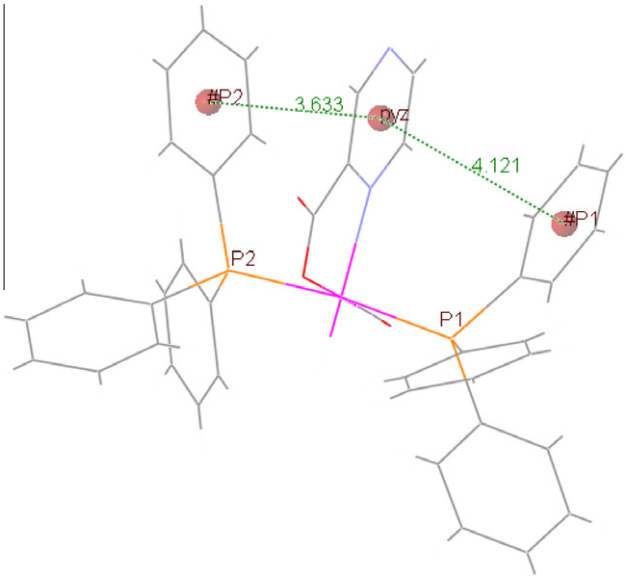

Fig. 2. The π-stacking interaction in the [RuH(CO)(pyzCOOH)(PPh_3)$_2$] (**1**) complex molecule.

group and water molecule respectively. The ^{1}H NMR spectra of the complexes present signals at high field (−9.514, −9.568 and −9.529 ppm) which indicate the presence of a hydride coordinated with the metal. The shifts of the signals are due to the shielding effect of the metal and to the charge of the hydrogen atom. The Ru–H signals are triplets due to coupling with the two *trans* equivalent phosphorus atoms ($J_{HP} \sim 19.4$ Hz).

The IR spectra of complexes **1** and **2** display strong C≡O bands at 1973 and 1958 cm^{-1}. In the IR spectrum of complex (**3**) two $\nu_{(CO)}$ stretching bands are present at 1947 and 1943 cm^{-1}. The differences in the vibration frequencies between the carbonyl groups bonded to the Ru(III) and Ru(II) ions are connected to the difference in bond orders in the carbonyl groups. The bond length in the carbonyl group bonded to ruthenium(II) is longer compared with the one at Ru(III). Moreover the inclusion of electron-acceptor ligands, such as chlorine, in the coordination sphere should produce an effect decreasing the electron density on the metal, and therefore increasing the bond order of the CO bond and increasing the vibration frequency. The electron–donor hydride ligand at the Ru(II) ion delivers electron density via backbonding to the

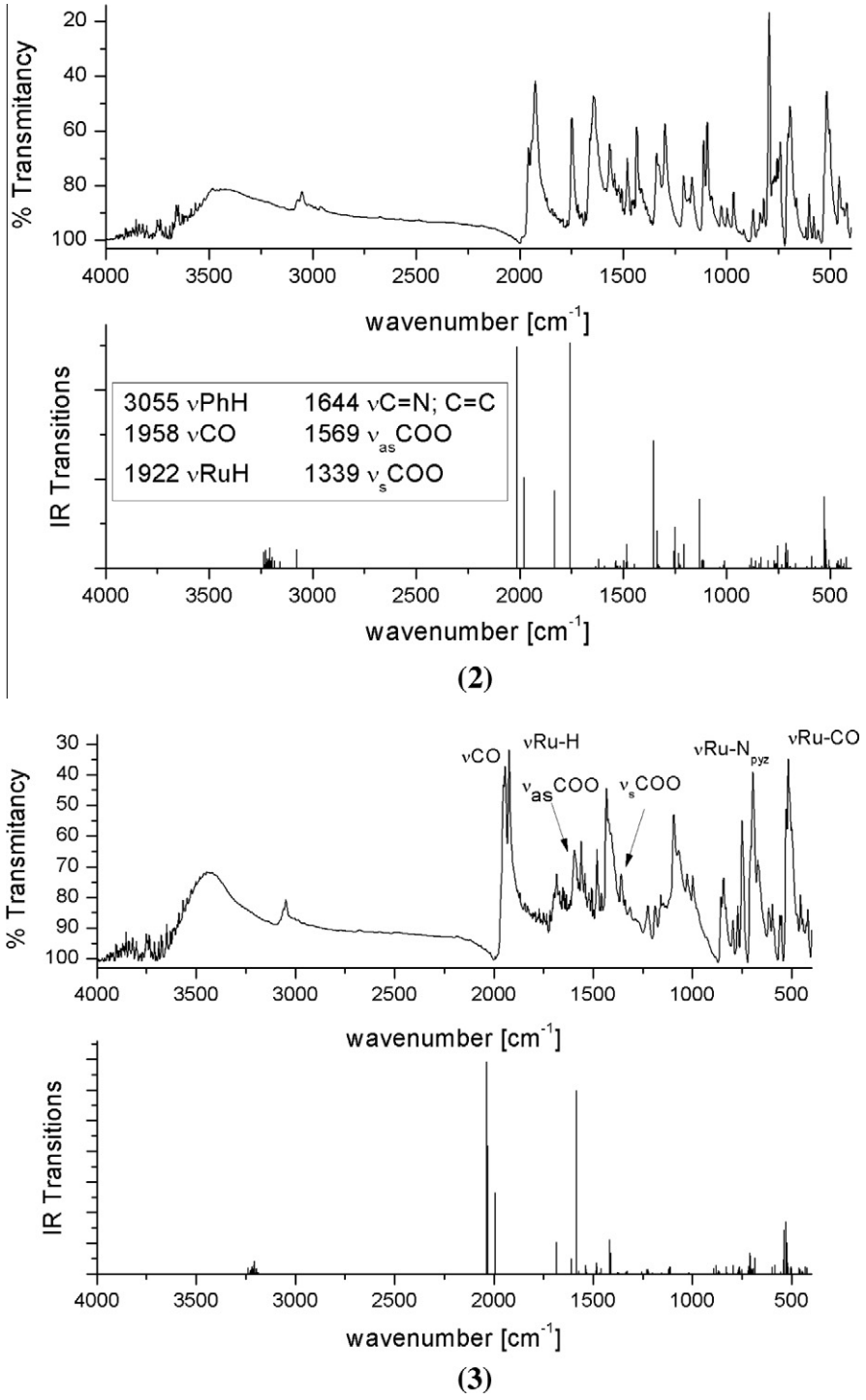

Fig. 3. IR spectra of the complexes $[RuH(CO)(pyz\text{-}2,3\text{-}COO[CH_3])(PPh_3)_2]\cdot H_2O$ (**2**) and $[Ru_2HCl_2(PPh_3)_3(pyz\text{-}2,3\text{-}COO)]$ (**3**).

anti-bonding orbitals of the CO ligand and produces a decrease of about 4 cm^{-1} in the vibration frequency of the CO bond [35]. The electronic effect is supported by theoretically determined charge values which indicate a more negatively charged Ru(II) central ion (−0.72) than Ru(III) (−0.26). The charge on the hydride ion is close to zero, (0.06) with a positive sign. Additionally the decrease of the CO vibration frequencies from 1973 to 1958 cm^{-1} in complexes **1** and **2** respectively indicates differences in the acceptor properties of pyrazine-2-carboxylic acid and pyrazine-2,3-dicarboxylic acid. In fact, by reducing the electron density on the metal carbonyl ligand, it will receive electron density via a $d\pi \rightarrow \pi^*$ interaction, which would increase the bond order, and in turn increase the vibration frequency of the CO bond. So it can be said that the dicarboxylic ligand behaves as a stronger acceptor with respect to the monocarboxylic derivative.

The ν_{CO} and ν_{Ru-H} stretching bands in the parent $[RuHCl(CO)(PPh_3)_3]$ complex are at 2020 and 1922 cm^{-1} respectively and the decrease of the carbonyl stretches are clearly visible in the studied complexes. The Ru–H stretching bands are displayed at 1928, 1922 and 1923 cm^{-1} in the spectra of complexes **1**, **2** and **3**, respectively. Stretching vibrations for C=C and C=N are observed in the 1593–1655 cm^{-1} range. The asymmetric and

Table 4
The occupancies and hybridization of the calculated R–H, Ru–C and C≡O natural bond orbitals (NBOs) of the complexes [RuH(CO)(pyzCOOH)(PPh_3)$_2$] (**1**), [RuH(CO)(pyz-2,3-COO[CH_3])(PPh_3)$_2$] (**2**) and [$Ru_2HCl_2(PPh_3)_3$(pyz-2,3-COO)] (**3**).

BD (2-center bond)	Occupancy	Hybridization of NBO	Wiberg bond indices
	Ru–H		
1	1.844 (0.121)	$0.723(sp^{0.64}d^{2.39})_{Ru} + 0.690(s)_H$	0.77
2	1.843 (0.121)	$0.725(sp^{0.63}d^{2.39})_{Ru} + 0.689(s)_H$	0.78
3	1.854 (0.112)	$0.727(sp^{0.61}d^{2.48})_{Ru} + 0.686(s)_H$	
	Ru–C		
1	1.945 (0.062)	$0.581(sp^{0.82}d^{2.60})_{Ru} + 0.814(sp^{0.50})_C$	1.35
2	1.944 (0.144)	$0.581(sp^{0.87}d^{2.63})_{Ru} + 0.814(sp^{0.50})_C$	1.35
3			
Ru(1)	1.946 (0.136)	$0.581(sp^{0.82}d^{2.60})_{Ru} + 0.813(sp^{0.52})_C$	1.34
Ru(2)	1.949 (0.132)	$0.576(sp^{0.68}d^{2.33})_{Ru} + 0.817(sp^{0.52})_C$	1.33
	C≡O		
1	1.996 (0.216)	$0.496(sp^{27.42})_C + 0.868(sp^{22.13})_O$	2.01
	1.995 (0.219)	$0.496(sp)_C + 0.868(p)_O$	
	1.992 (0.048)	$0.545(sp^{2.67})_C + 0.838(sp^{1.57})_O$	
2	1.996 (0.217)	$0.497(sp^{25.54})_C + 0.868(sp^{20.68})_O$	2.01
	1.995 (0.223)	$0.494(sp)_C + 0.869(sp^{33.33})_O$	
	1.992 (0.047)	$0.546(sp^{2.63})_C + 0.838(sp^{1.54})_O$	
3			
Ru(1)	1.996 (0.216)	$0.499(sp^{31.13})_C + 0.866(sp^{24.52})_O$	2.03
	1.994 (0.208)	$0.502(sp^{22.38})_C + 0.865(sp^{18.14})_O$	
	1.992 (0.054)	$0.545(sp^{2.80})_C + 0.838(sp^{1.65})_O$	
Ru(2)	1.996 (0.212)	$0.491(p)_C + 0.871(p)_O$	2.04
	1.996 (0.194)	$0.504(sp^{16.72})_C + 0.871(sp^{13.08})_O$	
	1.995 (0.043)	$0.547(sp^{2.55})_C + 0.837(sp^{1.57})_O$	

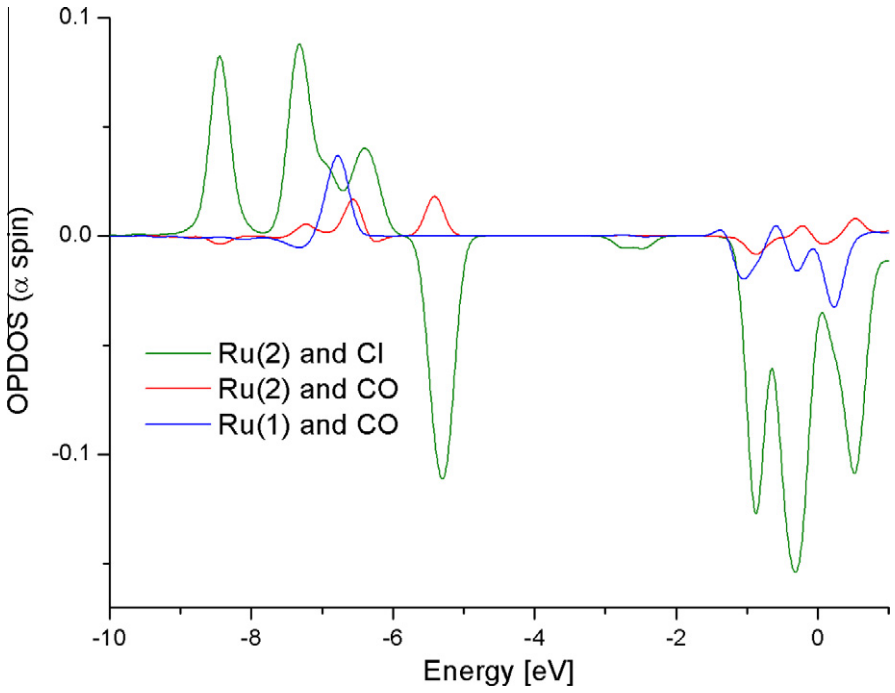

Fig. 4. Interactions between ruthenium atoms and carbonyl and chloride ligands in the complex [$Ru_2HCl_2(PPh_3)_3$(pyz-2,3-COO)] (**3**).

symmetric stretches of the COO groups gave bands with maxima in the ranges 1580–1559 and 1359–1339 cm^{-1} respectively.

3.2. Molecular structures

Crystals of the complexes suitable for single crystal X-ray analyses were obtained by slow evaporation of the reaction mixtures. The complexes **1** and **2** crystallize in the monoclinic $P2_1/n$ space group, and the dinuclear complex **3** in the triclinic $P\bar{1}$ space group. Complex **2** crystallizes as a solvate with one water molecule. Fig. 1 presents the molecular structures of the complexes and selected bond distances and angles are collected in Table 2. The structures of the complexes can be considered as distorted octahedral with the largest deviation from the expected 90° bond angles coming from the bite angle of the pyrazine carboxylic acid. It equals 76.41(9), 75.74(12) and 73.90(16), 75.06(17)° for the N–Ru–O angles in complexes **1**, **2** and **3** respectively. The P–Ru–P angles are lower than 180°, being in the 168.02(4)–173.03(3)° range. The *trans effect* of the H^- ligand is visible in an elongation of the Ru(1)–N(1) bond by about 0.04 Å compared to the Ru(2)–N(2) bond distance in the dinuclear complex **3**. Some differences in the bond lengths of the carbonyl group have been mentioned

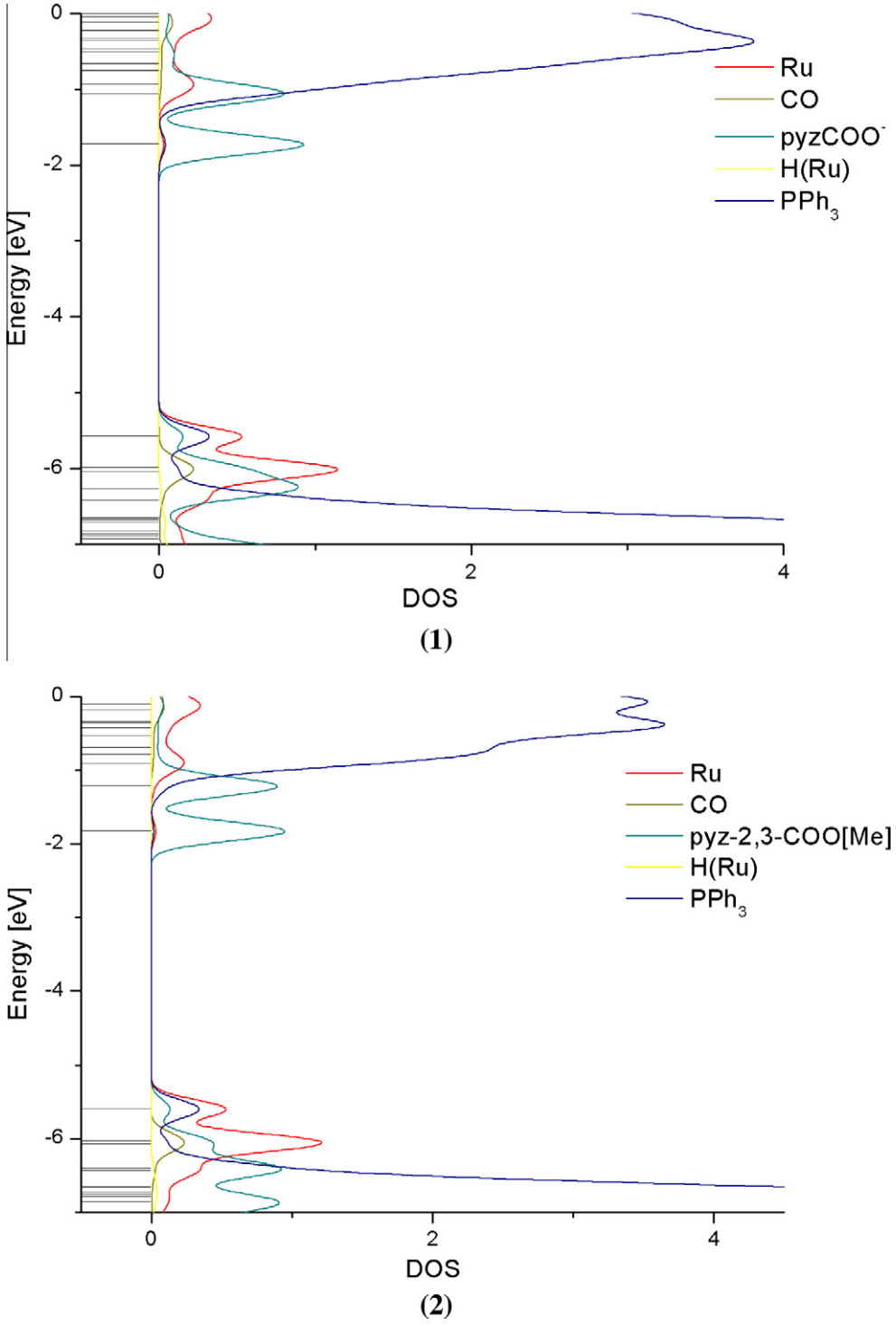

Fig. 5. The density of states (DOS) diagrams for complexes **1** and **2**.

earlier. As shown in Fig. 1, the CO groups are in *trans* positions to the carboxyl groups of pyrazine in the complexes. This configuration is preferred because of the donor/acceptor properties of the carboxyl and carbonyl groups. In the $[RuHCl(CO)(pyz)(PPh_3)_2]$ complex, the pyrazine occupies the *trans* position to the carbonyl ligand [36], which indicates an electronic reason for the configuration of the ligands about the ruthenium central ions in the complexes.

In the molecular structures of the complexes several weak inter- and intramolecular hydrogen bonds [37] exist, as collected in Table 3. Additionally, in the structure of the complexes some electronic interactions (π–π stacking) between the PPh_3 phenyl and pyrazine rings are visible. Fig. 2 presents the alignment of the centroids formed by the pyrazine and phosphine phenyl rings. The plane-to-plane distance between the #P2 centroid, determined by C(31) to C(36) carbons, and pyrazine ring is equal to 3.63 Å, indicating a π–π stacking interaction. The angle between the normal to #P2 and #pyz is 20.36°. It follows that the interaction between #P2 and #pyz is very weak. A similar arrangement of the phosphine phenyl and pyrazine rings occurs in the structures

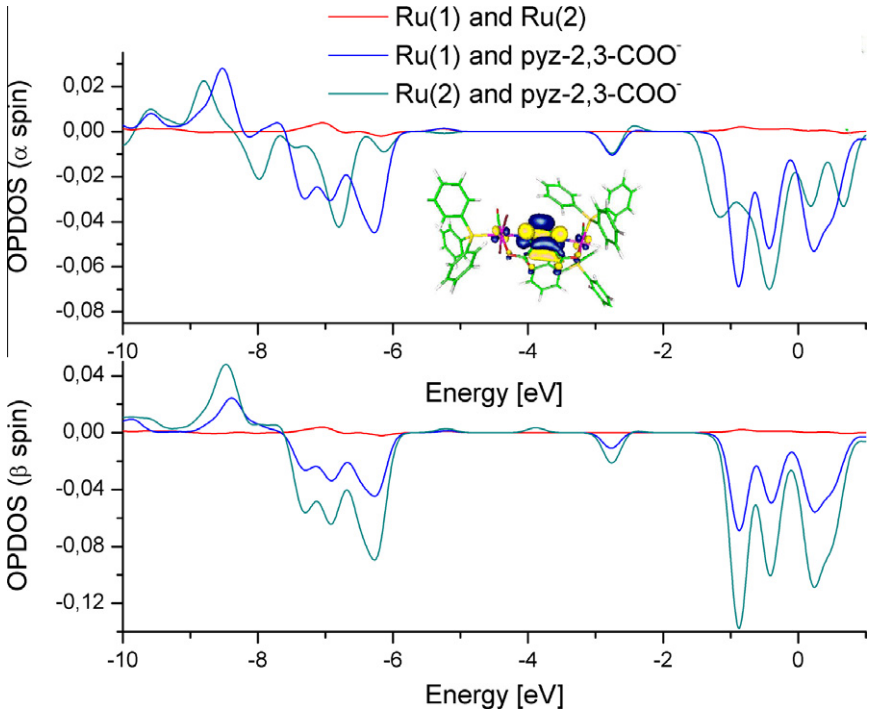

Fig. 6. The overlap partial density of states diagrams for the complex $[Ru_2HCl_2(PPh_3)_3(pyz\text{-}2,3\text{-}COO)]$ (**3**).

of other complexes. In the molecule of complex **2**, the distances between #P1 (C(21)–C(26)), #P2 (C(39)–C(44)) and the #pyz centroid are 3.79 and 3.70 Å and the angles are 21.08 and 18.30°, respectively. In the structure of the dinuclear complex **3** a similar arrangement occurs in the coordination sphere of ruthenium(II), with distances #P1–#pyz 3.81, #P2–#pyz 3.68 Å and angles equal to 14.33 and 15.37°. These intramolecular π–π interactions may explain the presence of singlet signals in the ^{31}P NMR spectra of compmlexes **1** and **2**. The P(1)–Ru(1)–P(2) angle of about 170° in the crystal structures changes to about 180° in solution by increasing the strength of the π–π interactions.

3.3. Optimized geometries, hybrid and molecular orbitals description

The ground states geometries of the studied complexes were optimized in singlet states in the case of complexes **1** and **2**, and in the doublet state for complex **3** using the DFT method with the B3LYP functional. The calculations were carried out for gas phase molecules and in general the predicted bond lengths and angles are in agreement with the values based on the X-ray crystal structure data. The general trends observed in the experimental data are well reproduced in the calculations. The calculated IR frequencies of complexes **2** and **3**, shown in Fig. 3, confirm the calculated structures with the experimental ones, and the differences in the calculated and experimental spectra mainly result from the negligence of intermolecular interactions for the gas phase. From the data collected in Table 2, one may see that the majority of differences between the experimental and calculated geometries are found in the Ru–P distances (~0.09 Å) and the angle differences do not exceed 6.5°. The C≡O bond lengths do not undergo important changes and maximally a slight increase of ~0.017 Å is seen for the carbonyl group at Ru(2) in complex **3**.

The NBO analyses were performed for the complexes, which allowed the nature of the coordination between ruthenium and the atoms of the ligands directly interacting with it to be known. This methodology also gave a better understanding of the optimized molecular structures. In the analysis it was found that the N,O–donor ligands do not show covalent bonding with ruthenium. Coulomb-type interactions between the ruthenium central ions and the pyrazine derivatives ligands are clearly visible in the calculated Wiberg bond indices, whose values are considerably lower than one. The Ru–N and Ru–O bond indices are similar and are close to 0.37 and 0.39 in complexes **1** and **2**, and are 0.37 and 0.36 (Ru^{2+}), 0.43 and 0.34 (Ru^{3+}) in **3**. The Ru–P bond orders are also smaller than 1 (0.7).

For the carbonyl groups of the investigated complexes, three natural bond orbitals were detected for the C–O bond, and one for the Ru–C bond. The Ru–C bond orbitals are polarized towards the carbon atom, and the C–O bond orbitals are polarized towards the oxygen end. The oxygen atom of the carbonyl ligand has one lone pair (LP) orbital. The occupancies and hybridization of the Ru–H, Ru–C and CO bonds are gathered in Table 4 (*anti*-bonding NBOs are given in round brackets). The charges of the CO ligands can be easily calculated by summing the individual charges on the carbon and oxygen atoms, and have values of 0.18 in complexes **1** and **2**, and 0.20 (Ru^{2+}) and 0.23 (Ru^{3+}) in **3**. These values show that there is some charge transfer between CO and the Ru fragment. The Wiberg indexes of the CO bonds in the complexes are reduced (by about 0.22) with respect to free CO (W_{CO} = 2.23). These weak values are in agreement with the elongation of the C–O bond in the complexes and the charge distribution in the terminal bonding carbonyl group to the ruthenium central ion. The bonding can be described as the result of two electron transfers. First this binding mode involves a σ-donation from the CO lone pair orbital to the LUMO orbital of complex. On the other hand, the highest occupied orbitals of the metallic fragment, mainly $4d_{Ru}$ orbitals, are involved in a π back-bonding from the metal to the CO π* orbitals. Additionally the charge on the carbonyl group bonded to the ruthenium(III) central ion in complex **3** has the highest positive value, which indicates the smallest charge transfer from metal to CO. This is consistent with crystallographic data in Table 2, where the C≡O bond length is only 1.145(8) Å. Fig. 4 shows the interaction between the ruthenium atoms and the carbonyl and chloride ligands in the complex $[Ru_2HCl_2(PPh_3)_3$

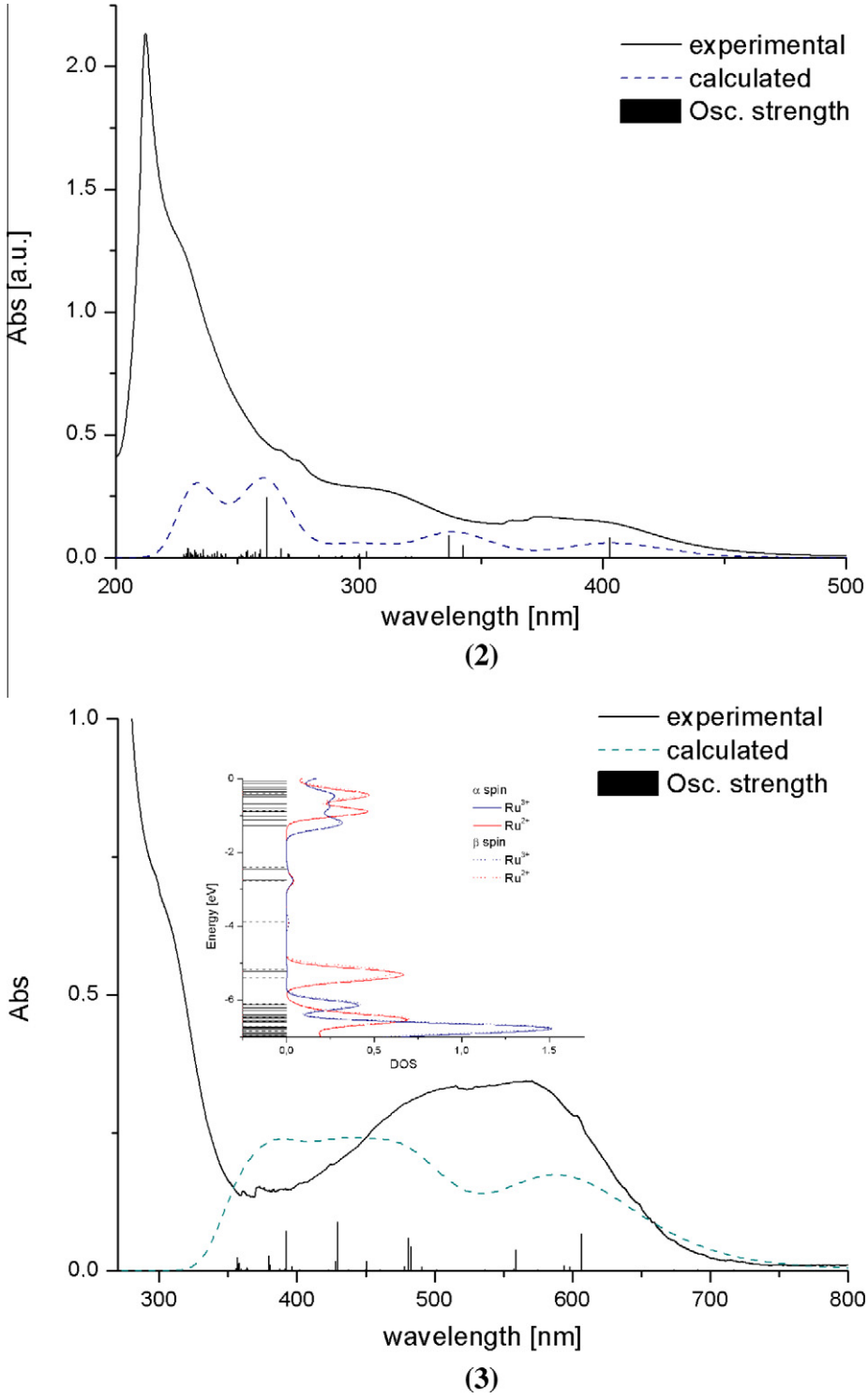

Fig. 7. Experimental and calculated UV–Vis spectra of the complexes [RuH(CO)(pyz-2,3-COO[CH_3])(PPh_3)$_2$]·H_2O (**2**) and [$Ru_2HCl_2(PPh_3)_3$(pyz-2,3-COO)] (**3**).

(pyz-2,3-COO)] (**3**). As one can see, the π-acceptor interaction between the carbonyl groups and ruthenium(III) is very small compared with the Ru(II)–CO interaction. However, a small transfer of electron density to the acceptor π^* carbonyl orbitals is compensated by the presence of the acceptor chloride ligands.

Analysis of the frontier molecular orbitals is useful for understanding spectroscopic properties, such as electronic absorption and emission spectra of organometallic complexes. The electronic structures of complexes **1** and **2** are similar because of the similar composition of their coordination spheres. The densities of states (DOS) in terms of Mulliken population analysis were calculated using the GAUSSSUM program, and Fig. 5 presents the composition of the fragment orbitals contributing to the molecular orbitals for complex **2**. The HOMOs are mainly localized on the ruthenium atoms (~53%) with a contribution from triphenylphosphine (~30%) and the pyrazine derivative ligands (~15%). The LUMOs are basically located in the pyrazine ligands. The d orbitals of the ruthenium central ions contribute in LUMO+2 (d_{z^2}) and LUMO+9/

Table 5
The calculated electronic transitions for the complex $[Ru_2HCl_2(PPh_3)_3(pyz\text{-}2,3\text{-}COO)]$ (**3**).

[nm]	*f*	Transitions	Charter
691.14	0.0022	H-7(β) → LUMO(β) (32%), H-3(β) → LUMO(β) (25%)	$d_{Ru(III)}/\pi_{Cl} \rightarrow d_{Ru}/\pi_{pyz}$
684.39	0.0	HOMO(α) → LUMO(α) (51%), HOMO(β) → L+1(β) (45%)	$d_{Ru}/\pi_{Cl} \rightarrow d_{Ru}/\pi_{pyz}$
673.75	0.0023	H-12(β) → LUMO(β) (19%), H-4(β) → LUMO(β) (37%)	$d_{Ru}/\pi_{PPh3} \rightarrow d_{Ru}/\pi_{pyz}$
660.65	0.0011	H-6(β) → LUMO(β) (18%), H-5(β) → LUMO(β) (33%)	$d_{Ru}/\pi_{PPh3} \rightarrow d_{Ru}/\pi_{pyz}$
606.42	0.0677	HOMO(α) → LUMO(α) (39%), HOMO(β) → L+1(β) (45%)	$d_{Ru(III)}/\pi_{Cl} \rightarrow d_{Ru}/\pi_{pyz}$
558.99	0.0385	H-1(α) → LUMO(α) (32%), H-1(β) → L+1(β) (47%)	$d_{Ru(III)}/\pi_{Cl} \rightarrow d_{Ru}/\pi_{pyz}$
557.48	0.0031	H-2(α) → LUMO(α) (35%), H-2(β) → L+1(β) (31%)	$d_{Ru(II)}/\pi_{PPh3} \rightarrow d_{Ru}/\pi_{pyz}$
536.75	0.0020	HOMO(β) → L+2(β) (89%)	$d_{Ru(III)}/\pi_{Cl} \rightarrow \pi_{pyz}$
501.29	0.0020	H-23(β) → LUMO(β) (77%)	$d_{Ru(III)}/\pi_{Cl} \rightarrow d_{Ru}/\pi_{pyz}$
490.91	0.0069	H-1(α) → L+1(α) (91%)	$d_{Ru(III)}/\pi_{Cl} \rightarrow d_{Ru}/\pi_{pyz}$
482.71	0.0437	H-1(β) → L+2(β) (66%)	$d_{Ru(III)}/\pi_{Cl} \rightarrow \pi_{pyz}$
480.91	0.0596	H-2(α) → LUMO(α) (36%), H-2(β) → L+1(β) (37%)	$d_{Ru(II)}/\pi_{PPh3} \rightarrow d_{Ru}/\pi_{pyz}$
478.20	0.0080	H-24(β) → LUMO(β) (76%)	$\pi_{PPh3} \rightarrow d_{Ru}/\pi_{pyz}$
450.57	0.0176	H-2(α) → L+1(α) (20%), H-2(β) → L+2(β) (63%)	$d_{Ru(II)}/\pi_{PPh3} \rightarrow d_{Ru}/\pi_{pyz}$
429.80	0.0994	H-29(β) → LUMO(β) (61%), H-28(β) → LUMO(β) (38%)	$\pi_{pyz} \rightarrow d_{Ru}/\pi_{pyz}$
396.65	0.0081	H-12(α) → LUMO(α) (10%), H-12(β) → L+1(β) (14%)	$\pi_{PPh3} \rightarrow d_{Ru}/\pi_{pyz}$
392.23	0.0723	H-31(β) → LUMO(β) (47%), H-29(β) → LUMO(β) (11%)	$d_{Ru(II)}/\pi_{PPh3}/\pi_{pyz} \rightarrow d_{Ru}/\pi_{pyz}$
387.401	0.0036	H-4(β) → L+1(β) (40%), H-3(β) → L+1(β) (19%)	$\pi_{PPh3}/\pi_{Cl} \rightarrow d_{Ru}/\pi_{pyz}$
379.80	0.0269	H-11(α) → LUMO(α) (14%), H-11(β) → L+1(β) (11%)	$d_{Ru(II)}/\pi_{PPh3} \rightarrow d_{Ru}/\pi_{pyz}$
366.52	0.001	H-15(α) → LUMO(α) (21%)	$\pi_{PPh3} \rightarrow d_{Ru}/\pi_{pyz}$
364.11	0.0039	H-15(β) → L+1(β) (19%)	$\pi_{PPh3}/\pi_{Cl} \rightarrow d_{Ru}/\pi_{pyz}$
363.79	0.0053	H-3(α) → L+1(α) (12%)	$\pi_{PPh3}/\pi_{Cl} \rightarrow d_{Ru}/\pi_{pyz}$

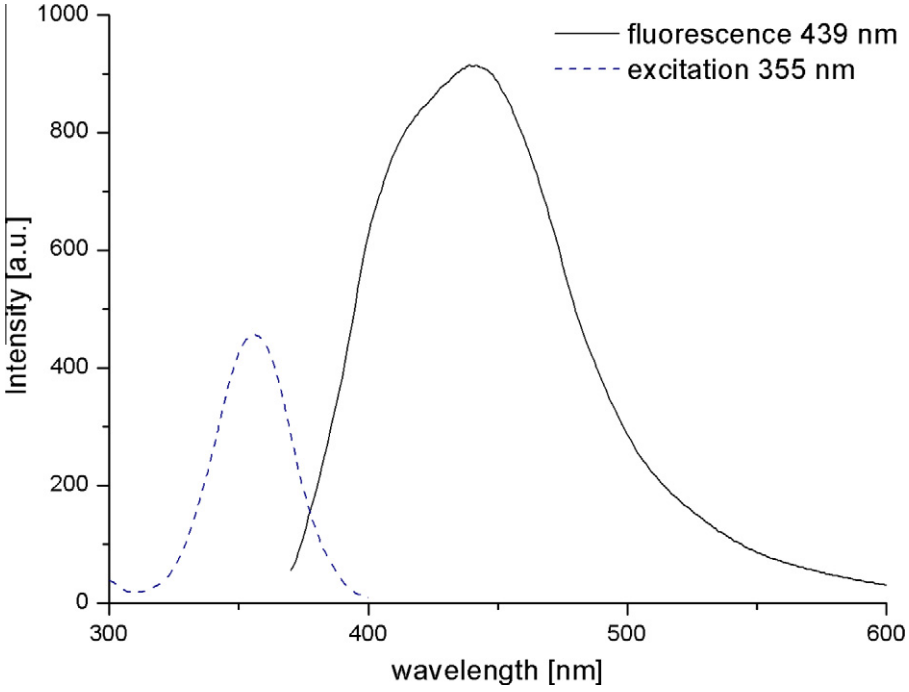

Fig. 8. The fluorescence spectrum of the complex $[RuH(CO)(pyz\text{-}2,3\text{-}COO[CH_3])(PPh_3)_2]\cdot H_2O$ (**2**) in methanolic solution ($c = 5 \times 10^{-4}$ mol/dm^3).

+10 ($d_{x^2-y^2}$) in complexes **1** and **2**. The carbonyl ligands play a significant role in the HOMO−1 and HOMO−2 orbitals. In the case of complex **3**, the LUMO is also localized on the pyrazine dicarboxylic ligand, with a contribution from the ruthenium(II) and (III) $d_{x^2-y^2}$ orbitals, indicating a weak interaction between the two ruthenium centers in the complex. The interaction is visible in Fig. 6 and, as one can see, the values of the Ru(II)–Ru(III) interaction in the energy range adequate for occupied and virtual molecular orbitals is small but positive, indicating some stabilizing interaction through the bridging pyrazine ligand.

3.4. Experimental and theoretical electronic spectra

The UV–Vis spectra of the monomeric complexes **1** and **2** are similar and maxima close to 360, 316 and 273 nm were measured. Based on the pseudooctahedral geometry of the complexes and taking into account d–d transitions assigned to $^1A_1 \rightarrow {}^1T_1$ and $^1A_1 \rightarrow {}^1T_2$ in an octahedral environment (or $^1A_1 \rightarrow {}^1A_2/B_1/E$ in lower symmetry fields), the ligand field parameter 10Dq can be estimated as 28469 and 28660 cm^{-1} for the complexes **1** and **2,** respectively. Racah's parameters are B = 248 and 279 cm^{-1}, and the nepheloauxetic parameters have values $\beta_{55} = 0.34$ and 0.39. The bands observed in the vicinity of 40 000 cm^{-1} (250 nm) have been attributed to intra- and interligand ($\pi^b_{C6H6} \rightarrow 3d_{phosphorus}$ and $\pi \rightarrow \pi_{C=C}$) transitions with an admixture of *Metal–Ligand Charge Transfer* transitions ($d_{Ru} \rightarrow \pi^*_{N\text{–}ligand}$ and $d_{Ru} \rightarrow \pi^*_{Ph}$). The highest experimental bands, close to 210.0 nm, may result from transitions in the PPh_3 ligands and from $\pi \rightarrow \pi^*$ excitations in the *N*-heteroaromatic ligands. Fig. 7 presents the experimental and calculated UV–Vis spectra of the complex [RuH(CO)

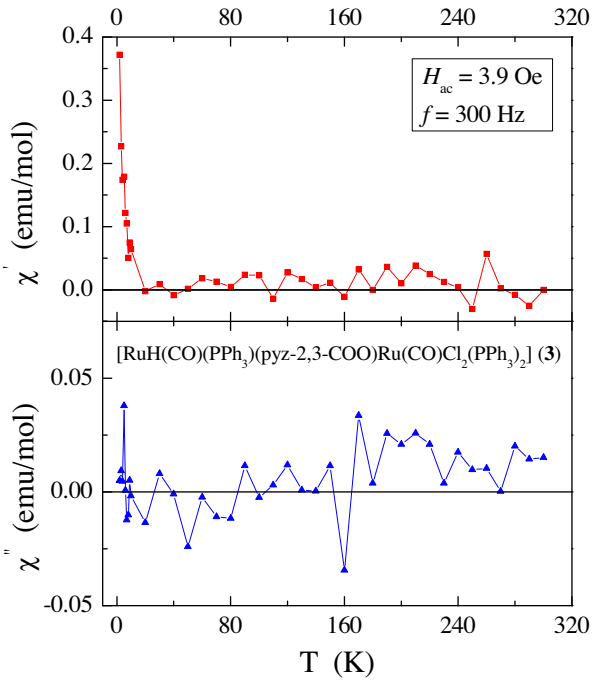

Fig. 9. In phase χ' and out of phase χ'' components of the dynamic susceptibility vs. temperature T for the complex [RuH(CO)(PPh_3)(pyz-2,3-COO)Ru(CO)Cl_2(PPh_3)$_2$] (**3**) recorded at an internal oscillating magnetic field H_{ac} = 3.9 Oe with an internal frequency f = 300 Hz.

(pyz-2,3-COO[CH_3])(PPh_3)$_2$] (**2**). The first band in the spectra of complexes **1** and **2** have HOMO/HOMO−1 → LUMO (98%/94%) character. As the frontier HOMOs are localized on the d ruthenium orbitals with an admixture of π–PPh_3, and the LUMOs are localised on the pyrazine derivative ligands, *Metal–Ligand Charge Transfer* transitions are associated with these orbital transitions. Higher energy bands (316, 273 nm) have been attributed to *Metal–Ligand Charge Transfer* transitions (d → $\pi^*_{PPh3/pyz}$). In this energy region, the transitions between HOMO−3 → LUMO (93%), HOMO−1 → LUMO+2 (53%) and HOMO → LUMO+5 (56%) were calculated.

The UV–Vis spectrum of complex **3** displays a broad band in the wavelengths range 700–400 nm. Analysis of this spectrum on the basis of terms due to two ruthenium central atoms with different oxidation states is difficult. It can be assumed that $^2T_{2g} \rightarrow {}^4T_{1g}$ and $^2T_{2g} \rightarrow {}^4T_{2g}$ transitions occur at longer wavelengths, and in the 500–400 nm range the $^2T_{2g} \rightarrow {}^2A_{1g}$, $^2T_{1g}$ transitions play a role with the MLCT (d → π^*_{quin}) and LMCT (π_{quin} → d) transitions. The UV–Vis spectrum of the complex was predicted by the TDDFT method and 90 electronic transitions are calculated. The experimental and calculated electronic spectra of the complex are presented in Fig. 7. The UV–Vis spectrum was calculated to only 355 nm, so the shortest wavelength experimental bands are not assigned to calculated transitions. Generally in the energy range considered, transitions were calculated between H-11(β), H-12(β), H-7(β), H-6(β) and HOMO(β) to LUMO(β) and at the shorter energies the H-1(α) → L+1(α) (91%) (490 nm) and H-2(α) → LUMO(α) (36%) (480 nm) transitions are visible. The transitions have d → d character with an admixture of π pyrazine and chloride orbitals. The participation of d ruthenium orbitals is shown in the DOS diagram in the inset of Fig. 7. Some calculated electronic transitions are presented in Table 5, and as can be seen, in most of the transitions the excitation of ruthenium(III) is involved. This is consistent with more electron density being localized on the Ru(III) atom as compared to Ru(II), associated with the weak donor interaction with the carbonyl group.

The emission characteristics of the complexes have been examined in methanol (for **1** and **2**) and dichloromethane (for **3**) solutions (with concentrations of 5×10^{-4} mol/dm^3) at room temperature. The excitations of complexes **1** and **2** were executed at a wavelength near to the maximum of the first electronic absorption. The excitation and emission spectra of complex **2** are presented in Fig. 8, and as can be seen, the excitation at 355 nm gave fluorescence with a maximum at 439 nm. The red shifts of the emission maximum of about 90 nm is typical for ruthenium(II) complexes and emissions originating from the lowest energy metal to ligand charge transfer (MLCT) state, derived from the excitation involving a $d_\pi \rightarrow \pi_{ligand}$ transition, are observed. The assignment is supported by the analysis of the frontier orbitals of the corresponding complexes, showing a contribution of ligand nature.

The excitation of complex **1** does not give any measurable emission, which confirms the MLCT nature of the fluorescence for complex **2**. As shown in the DOS diagrams presented in Fig. 5, the LUMO and LUMO+1 orbitals in complex **2** are localized mainly on the pyrazine ligand, in contrast to complex **1** where the ruthenium orbitals play a role in LUMO+1. The dichloromethane solution of complex **3** was excited in the range between 350 and 700 nm, and no emissions were observed, which is not surprising considering the electronic structure of the complex.

3.5. Magnetic properties

The ac magnetic susceptibility measurements for the complex [RuH(CO)(PPh_3)(pyz-2,3-COO)Ru(CO)Cl_2(PPh_3)$_2$] (**3**), displayed in Fig. 9, showed small values of the molar susceptibility, not exceeding 0.5 emu/mol at 2 K, a lack of a Curie-Weiss region and a weak magnetic interactions below 20 K, characteristic for a residual magnetism. In paramagnets, the Curie-Weiss law is obeyed, showing a hyperbolic temperature dependence of the susceptibility (cf. χ(T) in Ni [38] and Mn [39] complexes). The in-phase component χ'(T) is already fluctuating around zero above 20 K. It suggests that all the ions are diamagnetic. A fact that the energy is not being wasted for ordering and/or the reorientation of spins is also attesting to it, since the out of phase component, χ''(T) in Fig. 9 also fluctuates around zero. A small increase in χ'(T) below 20 K is probably connected with different electron density localized on the ruthenium ions.

4. Conclusion

Three new hydride-carbonyl complexes of ruthenium were synthesized and characterized by infra red, proton and phosphorus nuclear magnetic resonance, electronic absorption and emission spectroscopy and X-ray crystallography. The experimental studies were completed by theoretical calculations. The NBO calculations show that the donor properties of the carbonyl group predominate the π-acceptor ability in the ruthenium(III) complexes. The small transfer of electron density to the acceptor π^* carbonyl orbitals is compensated by the presence of acceptor ligands such as chloride. The theoretical results are in accordance with the experimental IR spectra and structural data. The donations from the ligands to the Ru(III) central ion in the [$Ru_2HCl_2(PPh_3)_3$(pyz-2,3-COO)] complex result in the final diamagnetism of the complex, as the ac magnetic susceptibility as well as the NMR studies have shown. The electronic structures of these complexes, presented in particular by the density of states diagrams, have been correlated with their ability to fluoresce and have been used to analyze the UV–Vis spectra.

Acknowledgement

Calculations have been carried out in Wroclaw Centre for Networking and Supercomputing (http://www.wcss.wroc.pl).

Appendix A. Supplementary data

CCDC 828260, 828261 and 829183 contains the supplementary crystallographic data for the complexes [RuH(CO)(pyzCOO)(PPh_3)$_2$] (**1**), [RuH(CO)(pyz-2,3-COO[CH_3])(PPh_3)$_2$]·H_2O (**2**) and [Ru_2HCl_2(CO)(pyz-2,3-COO)(PPh_3)$_3$] (**3**). These data can be obtained free of charge via http://www.ccdc.cam.ac.uk/conts/retrieving.html, or from the Cambridge Crystallographic Data Centre, 12 Union Road, Cambridge CB2 1EZ, UK; fax: +44 1223-336-033; or e-mail: deposit@ccdc.cam.ac.uk.

References

[1] L. Salvi, A. Salvini, F. Micoli, C. Bianchini, W. Oberhauser, J. Organomet. Chem. 692 (2007) 1442.
[2] C. Po Lau, S. Man Ng, G. Jia, Z. Lin, Coord. Chem. Rev. 251 (2007) 2223.
[3] C. Jun Yue, Y. Liu, R. He, J. Mol. Catal. A: Chem. 259 (2006) 17.
[4] F. Nipa Haque, A.J. Lough, R.H. Morris, Inorg. Chim. Acta 361 (2008) 3149.
[5] P. Buskens, D. Giunta, W. Leitner, Inorg. Chim. Acta 357 (2004) 1969.
[6] J. Bravo, J. Castro, S. Garcia-Fontana, M.C. Rodriguez-Martinez, G. Albertin, S. Antoniutti, A. Manera, J. Organomet. Chem. 692 (2007) 5481.
[7] M. Chandra, A.N. Sahay, D.S. Pandey, M.C. Puerta, P. Valerga, J. Organomet. Chem. 648 (2002) 39.
[8] A.K. Singh, P. Kumar, M. Yadav, D.S. Pandey, J. Organomet. Chem. 695 (2010) 567.
[9] M. Arias, J. Concepción, I. Crivelli, A. Delgadillo, R. Díaz, A. Francois, F. Gajardo, R. López, A.M. Leiva, L. Loeb, Chem. Phys. 326 (2006) 54.
[10] W. Henry, W.R. Browne, K.L. Ronayne, N.M. O'Boyle, J.G. Vos, J.J. McGarvey, J. Mol. Struct. 735–736 (2005) 123.
[11] B.J. Coe, S.J. Glenwright, Coord. Chem. Rev. 203 (2000) 5.
[12] C.R. Samanamú, A.F. Richards, Polyhedron 26 (2007) 923.
[13] R. Lalrempuia, P. Govindaswamy, Yurij A. Mozharivskyj, M. Rao Kollipara, Polyhedron 23 (2004) 1069.
[14] A. Skarżyńska, M. Siczek, Polyhedron 27 (2008) 1930.
[15] J.G. Małecki, A. Maroń, Polyhedron 30 (2011) 1225.
[16] J.G. Małecki, Polyhedron 30 (2011) 79.
[17] J.G. Małecki, Polyhedron 29 (2010) 2489.
[18] J.G. Małecki, R. Kruszyński, Z. Mazurak, Polyhedron 28 (2009) 3891.
[19] J.G. Małecki, R. Kruszyński, Z. Mazurak, J. Coord. Chem. 61 (2008) 2186.
[20] J.G. Małecki, R. Kruszyński, D. Tabak, J. Kusz, Polyhedron 26 (2007) 5120.
[21] J.G. Małecki, R. Kruszynski, Z. Mazurak, Polyhedron 26 (2007) 4201.
[22] J.G. Małecki, R. Kruszyński, Polyhedron 26 (2007) 2686.
[23] J.G. Małecki, R. Kruszyński, J. Coord. Chem 60 (2007) 2085.
[24] N. Ahmad, J.J. Levinson, S.D. Robinson, M.F. Uttely, Inorg. Synth. 15 (1974) 48.
[25] M.J. Frisch, G.W. Trucks, H.B. Schlegel, G.E. Scuseria, M.A. Robb, J.R. Cheeseman, G. Scalmani, V. Barone, B. Mennucci, G.A. Petersson, H. Nakatsuji, M. Caricato, X. Li, H.P. Hratchian, A.F. Izmaylov, J. Bloino, G. Zheng, J.L. Sonnenberg, M. Hada, M. Ehara, K. Toyota, R. Fukuda, J. Hasegawa, M. Ishida, T. Nakajima, Y. Honda, O. Kitao, H. Nakai, T. Vreven, J.A. Montgomery Jr., J.E. Peralta, F. Ogliaro, M. Bearpark, J.J. Heyd, E. Brothers, K.N. Kudin, V.N. Staroverov, R. Kobayashi, J. Normand, K. Raghavachari, A. Rendell, J.C. Burant, S.S. Iyengar, J. Tomasi, M. Cossi, N. Rega, J.M. Millam, M. Klene, J.E. Knox, J.B. Cross, V. Bakken, C. Adamo, J. Jaramillo, R. Gomperts, R.E. Stratmann, O. Yazyev, A.J. Austin, R. Cammi, C. Pomelli, J.W. Ochterski, R.L. Martin, K. Morokuma, V.G. Zakrzewski, G.A. Voth, P. Salvador, J.J. Dannenberg, S. Dapprich, A.D. Daniels, O. Farkas, J.B. Foresman, J.V. Ortiz, J. Cioslowski, D.J. Fox, GAUSSIAN 09, Revision **A.1**, Gaussian, Inc., Wallingford CT, 2009.
[26] A.D. Becke, J. Chem. Phys. 98 (1993) 5648.
[27] C. Lee, W. Yang, R.G. Parr, Phys. Rev. B 37 (1988) 785.
[28] K. Eichkorn, F. Weigend, O. Treutler, R. Ahlrichs, Theor. Chim. Acc. 97 (1997) 119.
[29] M.E. Casida, in: J.M. Seminario (Ed.), Recent Developments and Applications of Modern Density Functional Theory, Theoretical and Computational Chemistry, vol. 4, Elsevier, Amsterdam, 1996, p. 391.
[30] E.D. Glendening, A. E. Reed, J. E. Carpenter, F. Weinhold, NBO (version 3.1).
[31] N.M. O'Boyle, A.L. Tenderholt, K.M. Langner, J. Comp. Chem. 29 (2008) 839.
[32] CrysAlis RED, Oxford Diffraction Ltd., Version 1.171.29.2.
[33] O.V. Dolomanov, L.J. Bourhis, R.J. Gildea, J.A.K. Howard, H. Puschmann, J. Appl. Cryst. 42 (2009) 339.
[34] G.M. Sheldrick, Acta Cryst. A64 (2008) 112.
[35] J.G. Małecki, R. Kruszynski, J. Coord. Chem. 60 (2007) 2085.
[36] M. Yánez, J. Guerrero, P. Aguirre, S.A. Moya, G. Cárdenas-Jirón, J. Organomet. Chem. 694 (2009) 3781.
[37] G.R. Desiraju, T. Steiner, The Weak Hydrogen Bond in Structural Chemistry and Biology, Oxford University Press, 1999.
[38] J.G. Małecki, A. Świtlicka, T. Groń, M. Bałanda, Polyhedron 29 (2010) 3198.
[39] J.G. Małecki, B. Machura, A. Świtlicka, T. Groń, M. Bałanda, Polyhedron 30 (2011) 746.